Energy Conversion and Management 174 (2018) 417–429

Contents lists available at ScienceDirect

Energy Conversion and Management

journal homepage: www.elsevier.com/locate/enconman

# Thermal analysis and optimization of a system for water harvesting from humid air using thermoelectric coolers

M. Eslami[a,*], F. Tajeddini[b], N. Etaati[a]

[a] School of Mechanical Engineering, Shiraz University, Shiraz, Iran
[b] School of Mechanical Engineering, Sharif University of Technology, Tehran, Iran

ARTICLE INFO

*Keywords:*
Thermoelectric cooler
Atmospheric water generation
Thermodynamic optimization

ABSTRACT

Condensation of water vapor available in atmospheric air can be considered as a solution for water scarcity problem. In this paper, a comprehensive thermodynamic analysis of water production from humid air using thermoelectric coolers (TECs) is presented. The system consists of a number of thermoelectric coolers, a fan to supply the required air flow circulation, two cold and hot air channels, heat sinks and solar cells for powering the thermoelectric coolers and fan. Effects of various design parameters are investigated and discussed. The proposed design is optimized to get the maximum effectiveness which is defined as the amount of produced water per unit of energy consumption. Sensitivity analysis is used to find the optimum number of TECs, length of the channels and performance of the system at different temperatures. The resulting system is capable of producing 26 ml of water within 1 h from the air with 75% relative humidity and the temperature of 318 K by consuming only 20 W of electrical power. In addition, the annual performance and optimization of this device in three southern cities of Iran are presented based on hourly meteorological data. Finally, comparison of the present system with other air water generators indicates that the proposed design is the most energy efficient system among similar devices especially in high relative humidity.

## 1. Introduction

Nowadays, water scarcity is one of the most serious issues in the world. Approximately, around 97.5% of the water content of the earth is salty seawater which means only 2.5% of the existing water is fresh. Almost 70% of this amount is frozen at the polar ice caps, and around 30% exists in the form of moisture in the air or underground aquifers. Therefore, it can be concluded that only less than 1% of the earth's fresh water is accessible for direct human use [1]. Mekonnen et al. [2] notified that as many as four billion people all around the world face the problem of water scarcity for at least one month per year. All these factors have brought about the need to study solutions addressing the water scarcity problem.

Among different methods of desalination, atmospheric water generation (AWG) can be an easy method for fresh water production especially for places with high relative humidity. In this approach, ambient air is cooled down below the dew point temperature and the condensed water is collected. Vapor compression refrigeration, absorption refrigeration and thermoelectric cooling (TEC) can be used for this purpose. Thermoelectric coolers are devices which function on the basis of Peltier effect. By passing an electric current through them, they produce a temperature difference resulting in a cooling effect. In comparison with vapor compression and absorption refrigeration, TEC devices have no moving parts and require less maintenance. Therefore, they are suitable for designing simple and portable AWG systems. However, the designer must be very careful about the performance and efficiency of TECs at various operating conditions.

There are different approaches to study properties and modeling the behavior of thermoelectric coolers [3–7]. Zhao and Tan [3] presented a study of material, modeling, and application of thermoelectric coolers. Fraisse et al. [4] compared different methods of modeling TECs. Also, Mani [5] studied the behavior of thermoelectric coolers numerically and analytically and revealed that the results of these two approaches are in good agreement.

The coefficient of performance is among the most important topics related to thermoelectric coolers. For this purpose, Enescu and Virjoghe [6] provided a review of thermoelectric cooling parameters and performance. In addition, Xuan [7] investigated the effect of thermal and contact resistance of thermoelectric coolers. Based on his studies, the amount of COP depends on thermoelectric length. Also by increasing the thermal contact resistance, this dependence increases significantly.

The maximum COP of a TEC device in both cooling and heating

* Corresponding author.
*E-mail address:* meslami@shirazu.ac.ir (M. Eslami).

https://doi.org/10.1016/j.enconman.2018.08.045
Received 25 April 2018; Received in revised form 2 August 2018; Accepted 12 August 2018
Available online 20 August 2018
0196-8904/ 

**Nomenclatures**

| | |
|---|---|
| $A_c$ | cross section area of a fin ($m^2$) |
| $A_f$ | fins area ($m^2$) |
| $A_t$ | total area ($m^2$) |
| $C_p$ | specific heat (kJ/kg K) |
| COP | coefficient of performance |
| D | diameter (m) |
| *Eff* | effectiveness (L/J) |
| *f* | fraction factor |
| *h* | enthalpy (J/kg) |
| $h_{conv}$ | convection heat transfer coefficient ($W/m^2$ K) |
| H | height of each channel's hole (m) |
| *I* | current (A) |
| $k_f$ | thermal conductivity of base air flow (W/m K) |
| $k_s$ | thermal conductivity of base plate material (W/m K) |
| $K_m$ | TEC module thermal conductance (W/K) |
| l | length (m) |
| $l_c$ | characteristic length (m) |
| N | number |
| *Nu* | Nusselt number |
| *p* | perimeter (m) |
| *P* | power (W) |
| *Pr* | Prandtl number |
| *Q* | transferred heat (W) |
| *R* | resistance (K/W) |
| *R″* | thermal resistance ($m^2$ K/W) |
| $R_m$ | TEC module electrical resistance (ohm) |
| *Re* | Reynolds number |
| $S_m$ | TEC module Seebeck coefficient (V/K) |
| T | thickness (m) |
| *T* | temperature (K) |
| *u* | air velocity (m/s) |
| *V* | voltage (V) |
| $\dot{V}$ | volume flow rate of water (L/s) |
| w | width (m) |

*Greek symbols*

| | |
|---|---|
| $\eta_0$ | overall surface efficiency |
| $\eta_f$ | efficiency of fin with an adiabatic tip |
| $\nu$ | kinematic viscosity ($m^2/s$) |
| $\Delta P$ | pressure drop (Pa) |
| $\Delta T$ | temperature difference (K) |
| ρ | density ($kg/m^3$) |
| $\phi$ | relative humidity |
| $\omega$ | humidity ratio |

*Subscripts*

| | |
|---|---|
| a | ambient |
| c | cold side |
| equ | equivalent resistance |
| h | hot side |
| hyd | hydraulic |
| LMTD | log mean temperature difference |
| max | maximum |
| opt | optimum |
| *t*, *b* | resistance of the un-finned part of the heat sink |
| *t*, *base* | thermal resistance of the base surface |
| *t*, *c* | contact resistance |
| | resistance of the extended surfaces |
| TEC, m | thermoelectric cooler |
| w | water |

mode is one of the important issues that should be considered. Cosnier et al. [8] examined the performance of thermoelectric coolers by experimental and numerical analysis and revealed that it is possible to reach the coefficient of performances above 1.5 for cooling mode, and 2 for heating mode. Also, Liu et al. [9] used thermoelectric coolers for various air conditioning applications and showed that it is possible to reach the COP of 2.59 for cooling mode and 3.01 for heating mode. These results suggest that TEC devices can be a good choice for water harvesting if they are used efficiently.

Reducing the hot side temperature of a thermoelectric cooler is an approach to increase the coefficient of performance. For example, Sadighi Dizaji et al. [10] used water flow for cooling the hot side of a TEC instead of air and showed that it is possible to increase the cold side performance of TEC significantly. Seo et al. [11] studied the effect of different heat sink's shapes on the performance of TECs, numerically and showed the shape of heat sinks can change the operating performance of thermoelectric coolers. Also Via'n and Astrain [12] designed a heat sink for the cold side of a TEC and showed that by using this heat sink, COP can increase up to 32%. In addition, Zhu et al. [13] studied the effect of different heat exchanger sizes on the performance of TECs theoretically. According to their studies, the highest amount of COP is achieved by using the optimal heat sink size.

Another important parameter that significantly affects the performance of a TEC is the electrical current. Tan et al. [14] applied the second law of thermodynamics and showed that the amount of current must be precisely determined to achieve the optimal cold side temperature. Also Tan and Fok [15] presented an approach to analyze and optimize a thermoelectric cooling system.

The application of TECs in water harvesting from air is reported in several experimental studies [16–24]. Vian et al. [16] designed a device which was able to condense 0.969 L of water from the air in each day. Furthermore, Jradi et al. [17] theoretically and experimentally studied a system including 5 channels with 20 thermoelectric coolers in each powered by solar cells. This device is combined with a solar distiller humidifying ambient air to increase distillate output of water production. They showed that it is possible to produce 10 L of water during a summer day in Beirut. In another study, Yao et al. [18] produced 33.1 g/h of water by using a dehumidification device having more heat sinks on the two sides of thermoelectric coolers. In addition, Atta [19] designed a prototype including three TEC elements and a photovoltaic cell. He applied this system in Yanbu climate conditions and could produce almost 1 Liter of condensed water per hour. Besides, Joshi et al. [20] installed 10 TEC in a channel with the length of 70 cm and tested it in several different climate conditions. Based on this design, they harvested 240 ml of water in 10 h at a relative humidity of 90% and mass flow rate of 25 g/s. Tan and Fok [21] designed an AWG system and investigated the effect of input power to TECs and inlet mass flow rate on the amount of produced water. They revealed that it is possible to produce 50 ml of water in 3 h in an average relative humidity of 77%. Also, Liu et al. [22] built a portable water generator with two thermoelectric coolers and investigated the effect of inlet air relative humidity and air flow rates and showed that the maximum amount of generated water is 25.1 g per hour with 58.2 W input power. Munoz-Garcia et al. [23] designed a similar system for irrigation of young trees. Based on this design, they could harvest 35 ml water per hour from the air. Moreover, Pontious et al. [24] could harvest 0.21 L of water in a day with 0.33 kWh of energy consumption.

Recently, Shourideh et al. [25] performed a theoretical and experimental analysis of a Peltier AWG by optimizing the cold side extended surface and the cooling system. But they didn't investigate the

effect of thermal resistances and other parameters like the number of TECs in the optimization. They also compared the energy consumption of their design with some other AWG systems and showed that their system has a better performance. Besides, Salek et al. [26] performed a thermodynamic optimization for a solar driven ammonia absorption refrigeration cycle used for air dehumidification combined with a saline water desalination cycle.

The above literature review shows that most of the researches on thermoelectric AWG systems published so far are experimental and no comprehensive analytical solution and optimization for water harvesting by TECs has been provided. Therefore, this article tries to present a complete thermodynamic analysis of water production from humid air using TECs by considering effects of various design parameters, including thermal resistances and fins geometry. The resulting solution provides the necessary information to find the optimum number of TECs, length of the channel, electrical current and air mass flow rate. The objective is to maximize the amount of water production per unit power consumption of the fan and thermoelectric coolers in different operating conditions. Besides, the possibility of water production at different atmospheric conditions (relative humidity and temperature) can be predicted. Hence, the idea of using a controller to turn the device on and off is also investigated to decrease the power consumption while producing the same amount of water. As case studies, the annual performance of the device is investigated for three southern cities in Iran. These locations are typical examples of places with high relative humidity but very low annual rainfall.

## 2. System description

As shown in Figs. 1 and 2, the system considered in this article consists of a number of thermoelectric coolers placed in series. Air flows through two channels on the hot and cold sides and heat sinks increase the surface of heat transfer. A fan supplies the required air flow circulation and solar cells power the thermoelectric coolers and the fan.

The temperature distribution on the surface of the channels on both sides of the thermoelectric cooler is assumed to be uniform. The distance between two neighboring thermoelectric coolers is considered to be 1.5 cm to make this assumption reasonable. The entering air stream first passes through the channel on which the cold side of the thermoelectric coolers are placed, and after being cooled and dehumidified, goes through the warm channel and cools the hot side of thermoelectric cooler. Fig. 2 shows a schematic representation of the TECs inside channels.

Also, Table 1 presents the specifications of the thermoelectric cooler in this study.

## 3. Governing equations

Each thermoelectric cooler is identified by four basic characteristics including $I_{max}$, $V_{max}$, $\Delta T_{max}$ and $Q_{max}$. Along with the hot side temperature of a TEC ($T_h$), the parameters required for modeling thermoelectric coolers are defined, as follows [10,28]:

$$S_m = \frac{V_{max}}{T_h} \tag{1}$$

$$R_m = \frac{(T_h - \Delta T_{max})V_{max}}{T_h I_{max}} \tag{2}$$

$$K_m = \frac{(T_h - \Delta T_{max})V_{max} I_{max}}{2T_h \Delta T_{max}} \tag{3}$$

where $S_m$ is the Seebeck coefficient, $R_m$ is electrical resistance and $K_m$ is thermal conductivity.

By applying energy balance for a thermoelectric cooler, the cooling power and the heat released from the hot side of the thermoelectric cooler can be calculated [10,28]:

$$Q_c = S_m I T_c - \frac{I^2 R_m}{2} - K_m \Delta T \tag{4}$$

$$Q_h = S_m I T_h + \frac{I^2 R_m}{2} - K_m \Delta T \tag{5}$$

In these equations, $I$ is the electric current, $T_c$ is the cold side temperature of TEC, $T_h$ is the hot side temperature of TEC, $Q_c$ is the cooling power, $Q_h$ is the amount of heat dissipated from the hot side of TEC and $\Delta T$ is the temperature difference between hot and cold side of thermoelectric cooler:

$$\Delta T = T_h - T_c \tag{6}$$

On the other hand, the first law of thermodynamic gives:

$$P_{TEC} = Q_h - Q_c \tag{7}$$

where $P_{TEC}$ is thermoelectric power consumption. Combining Eqs. (4)–(7):

$$P_{TEC} = S_m I \Delta T + I^2 R_m \tag{8}$$

Also, the coefficient of performance of the thermoelectric cooler is defined as:

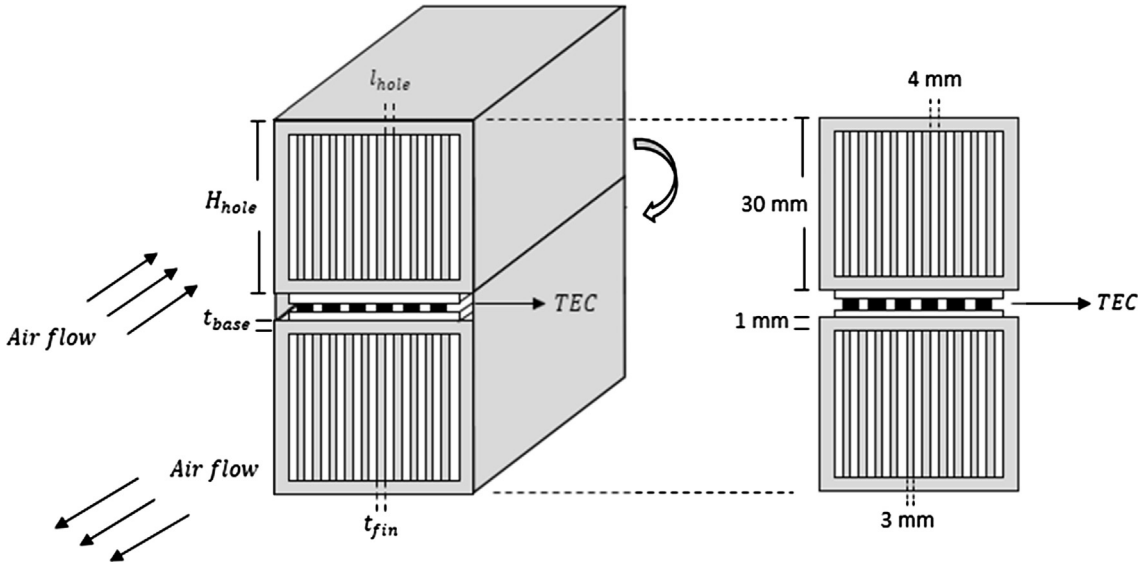


**Fig. 1.** A schematic of the system under study.

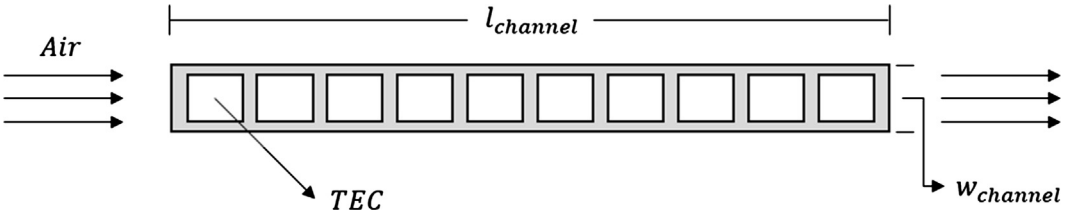


**Fig. 2.** The layout of thermoelectric coolers and the air passages over them.

**Table 1**
Thermoelectric cooler specifications KRYOTHERM TB-127-2,0-1,05(62) [27].

| Parameter | Value | Unit |
|---|---|---|
| $I_{max}$ | 17.6 | A |
| $V_{max}$ | 15.7 | V |
| $Q_{max}$ | 171.0 | W |
| $\Delta T_{max}$ | 69.0 | K |
| $l_{TEC}$ | 62.0 | mm |
| $w_{TEC}$ | 62.0 | mm |

$$COP = \frac{Q_c}{P_{TEC}} \tag{9}$$

The heat transfer between the air and the TECs in the channels is clearly related to the enthalpy change as follows:

$$Q_c = \dot{m}_c(h_{air\_in\_c} - h_{air\_out\_c}) \tag{10}$$

$$Q_h = \dot{m}_h C_{p\_h}(T_{air\_out\_h} - T_{air\_in\_h}) \tag{11}$$

where $C_p$ is the specific heat of air across the hot channel and $h$ is the enthalpy of humid air, in J/kg, which itself is a function of specific humidity $\omega$ [29]:

$$h = C_p(T-273) + \omega(2501.3 + 1.86(T-273))*1000 \tag{12}$$

As no water condensation occurs in the hot channel, the specific humidity of the air does not change so the enthalpy changes, $\Delta h$, can be replaced by $C_p \Delta T$ to calculate heat dissipated by the air in Eq. (11). In addition, since the hot side of TEC is cooled by the air discharge from the cold channel, then $T_{air\_in\_h} = T_{air\_out\_c}$.

The heat transfer in the channels can also be related to the temperature difference between the air stream and the hot and cold surfaces by LMTD method [30]:

$$Q_c = \frac{\Delta T_{LMTD\_coldside}}{R_c} \tag{13}$$

$$Q_h = \frac{\Delta T_{LMTD\_hotside}}{R_h} \tag{14}$$

$$\Delta T_{LMTD\_coldside} = \frac{[(T_{air\_out\_c} - T_c) - (T_a - T_c)]}{\ln\left(\frac{T_{air\_out\_c} - T_c}{T_a - T_c}\right)} \tag{15}$$

$$\Delta T_{LMTD\_hotside} = \frac{[(T_h - T_{air\_in\_h}) - (T_h - T_{air\_out\_h})]}{\ln\left(\frac{T_h - T_{air\_in\_h}}{T_h - T_{air\_out\_h}}\right)} \tag{16}$$

In Eqs. (13) and (14), parameters $R_c$ and $R_h$ are the total thermal resistance between the TEC surface and air flow in the cold and hot channels respectively. They can be calculated by adding different thermal resistances as shown in Fig. 3:

In Fig. 3, $R_{t,c}$ is the contact resistance between thermoelectric coolers and the heat sink attached to the cold channel. It can be modeled using the following expression:

$$R_{t,c} = \frac{R'_{t,c}}{N_{TEC} l_{TEC} w_{TEC}} \tag{17}$$

$N_{TEC}$ is the number of thermoelectric coolers and $l_{TEC}$ and $w_{TEC}$ are the length and width of each TEC, respectively. $R_{t,base}$ is the thermal resistance of the base surface on which thermoelectric coolers are installed and is calculated as follows:

$$R_{t,base} = \frac{t_{base}}{k_s l_{channel} w_{channel}} \tag{18}$$

where $t_{base}$, $l_{channel}$ and $w_{channel}$ are illustrated in Figs. 1 and 2 and $k_s$ is the thermal conductivity of base plate material.

The convection heat transfer resistance of the un-finned part of the heat sink $R_{t,b}$ can be combined with resistance of the extended surfaces $R_{t,f(N)}$ as an equivalent resistance $R_{equ}$. Assuming the lateral surfaces of the channel to be insulated [30]:

$$R_{equ} = \frac{1}{\eta_0 A_t h_{conv}} \tag{19}$$

In this equation, $\eta_0$ is the overall efficiency of the heat sink, given by [30]:

$$\eta_0 = 1 - \frac{N_{fin} A_f}{A_t}(1-\eta_f) \tag{20}$$

$$A_f = 2 w_{fin} l_c \tag{21}$$

$$l_c = l_{fin} + \frac{t_{fin}}{2} \tag{22}$$

$$A_t = l_{hole} l_{channel} N_{hole} + (2N_{hole} - 2) H_{hole} l_{channel} \tag{23}$$

where $N_{fin}$, $A_f$, $A_t$, $l_c$, and $N_{hole}$ are the number of fins, the fin area, the total area of heat transfer, equivalent fin length and the number of air passages, respectively. Also, $H_{hole}$ and $l_{hole}$ are shown in Fig. 1 and $l_{fin}$,

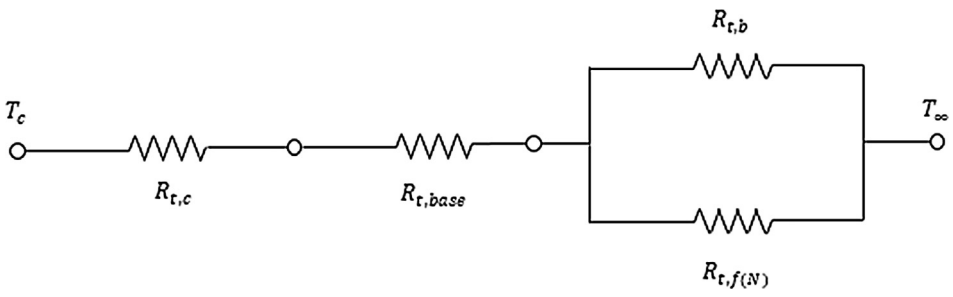


**Fig. 3.** Thermal resistances between the cold side of TEC and air flow in the channel.

$w_{fin}$ and $t_{fin}$ are illustrated in Fig. 4.

Assuming that the fin tips are adiabatic, $\eta_f$ is given by [30]:

$$\eta_f = \frac{\tanh ml_c}{ml_c} \tag{24}$$

in which,

$$m = \sqrt{\frac{h_{conv}p}{k_s A_c}} \tag{25}$$

$$p = 2(w_{fin} + t_{fin}) \tag{26}$$

$$A_c = w_{fin} t_{fin} \tag{27}$$

where $p$ is the perimeter and $A_c$ is the cross section area of a rectangular fin.

Also, the convection heat transfer coefficient $h$, in Eqs. (19) and (25), is calculated from the Nusselt number:

$$h_{conv} = \frac{Nuk_f}{D_{hyd}} \tag{28}$$

In which, $k_f$ is the thermal conductivity for air. Assuming turbulent flow, for both cooling and heating channels [30]:

$$Nu = 0.023Re^{0.8}\,Pr^{0.3} \quad for\ \ cooling \tag{29}$$

$$Nu = 0.023Re^{0.8}\,Pr^{0.4} \quad for\ \ heating \tag{30}$$

where $Pr$ is the Prandtl number and $Re$ is the Reynolds number defined as follows:

$$Re = \frac{u_{average}D_{hyd}}{\nu} \tag{31}$$

$$u_{average} = \frac{\dot{m}_a/N_{hole}}{\rho l_{hole}H_{hole}} \tag{32}$$

Also, in Eqs. (28) and (31), the characteristic length is hydraulic diameter $D_{hyd}$ that is given by:

$$D_{hyd} = \frac{4A_{hole}}{p_{hole}} = \frac{4l_{hole}H_{hole}}{2(l_{hole} + H_{hole})} \tag{33}$$

Finally, the total resistance is obtained:

$$R = R_{t,c} + R_{t,base} + R_{equ} \tag{34}$$

With the same procedure for hot channel, $R_h$ is calculated. Besides, the rate of water production in L/s is obtained using the following mass balance equation for water:

$$\dot{V}_w = \dot{m}_a(\omega_{air_{in_c}} - \omega_{air_{out_c}})\frac{1000}{\rho_{average}} \tag{35}$$

in which, $\rho_{average}$ is the density of water at the temperature of $\frac{T_{air\_out\_c} + T_{air\_in\_c}}{2}$.

To calculate the required fan power, pressure drop across the air passage is required [30]:

$$\Delta p = f\frac{\rho u_{average}^2}{D_{hyd}} l_{channel} \tag{36}$$

$$f = (0.790\ln(Re) - 1.64)^{-2} \tag{37}$$

Dimensions of the channel are chosen to have a turbulent flow for better heat transfer. Having $\Delta p$, the fan power consumption is given by [30]:

$$P_{fan} = \frac{\dot{m}}{\rho}\Delta p \tag{38}$$

## 4. Solution procedure

By considering the relative humidity of the outlet air from the cold channel to be equal to 100% and solving Eqs. (1)–(38), the values of power for the fan and thermoelectric coolers and also the amount of produced water are obtained. It should be noted that if the amount of produced water becomes negative, it means that the assumption of saturated air at the outlet is incorrect. In this case, instead of using this assumption, the condition $\omega_{air_{in_c}} = \omega_{air_{out_c}}$ is used, in order to obtain correct results. Fig. 5 shows a flow chart of different steps in the solution.

The geometrical and thermophysical properties of the present system are given in Table 2.

### 4.1. Validation

At first, the performance of the TEC modeled using Eqs. (1)–(9) is compared with results of the software provided by the thermoelectric manufacturer (KRYOTHERM) [27]. For $T_h = 300$ K, and $\Delta T = 20$ K and 40 K, changes of COP and $Q_c$ relative to the electric current is presented in Figs. 6 and 7. These results approve the accuracy of analytical equations used for modeling the thermoelectric cooler.

In the next step, the present model is used to simulate the experiments of Jradi et al. [17]. Fig. 8 illustrates the amount of water produced at different air flow rates for the electrical current of 2.6 A. Results show the maximum error of 6% compared to the experimental data and simulation results of Jradi et al. [17]. Also, effects of changing the electrical current for the fixed air flow rate of 0.0155 kg/s is shown in Fig. 9 which validates the accuracy of the present simulations.

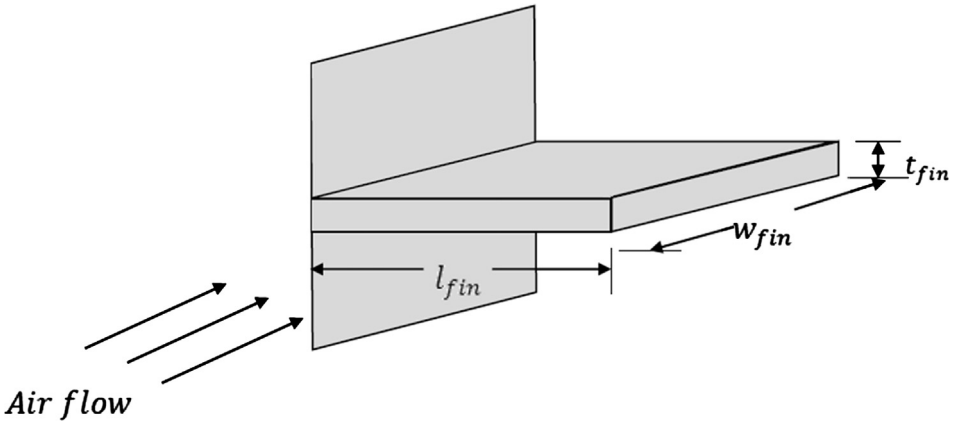


**Fig. 4.** A schematic of fin sizing.

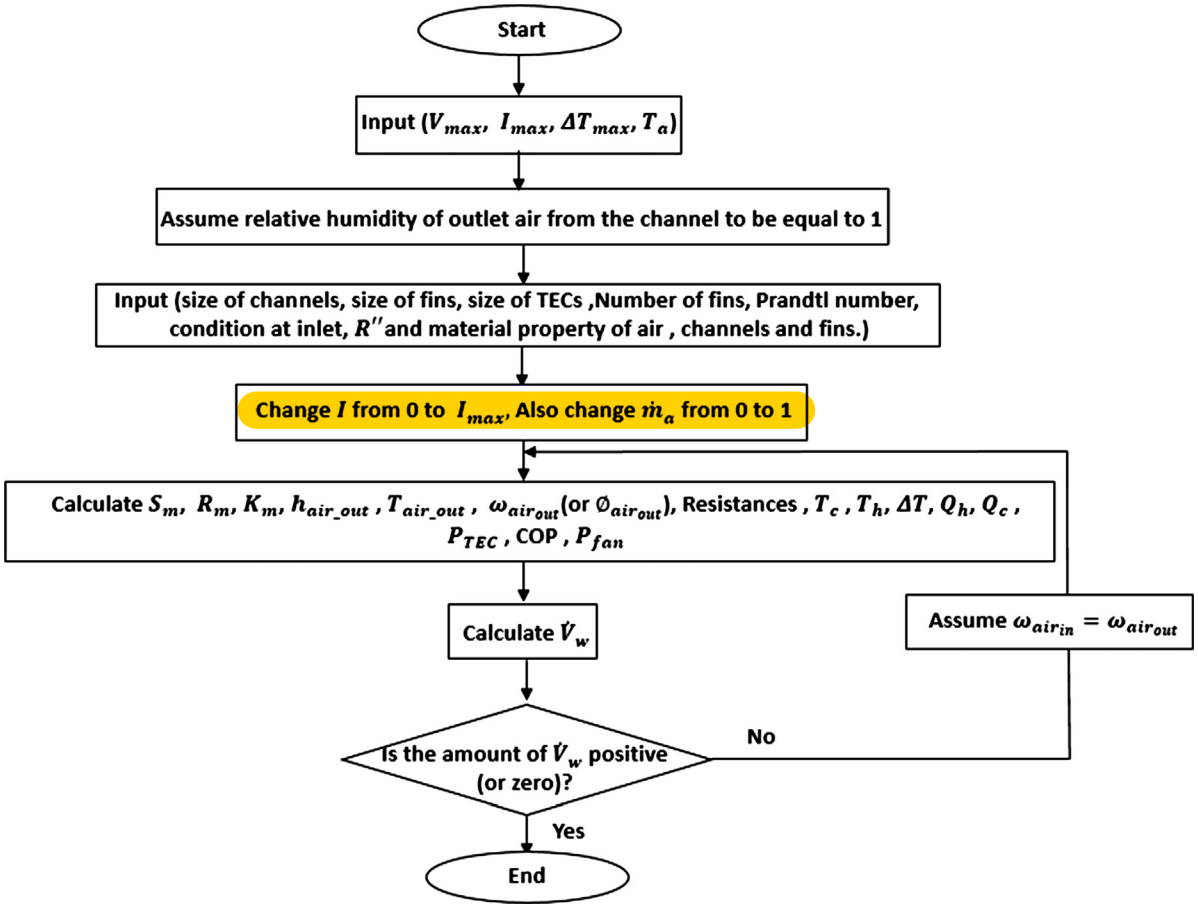


**Fig. 5.** The solution procedure.

**Table 2**
Fixed parameters needed to solve the problem.

| Parameter | Value | Unit |
|---|---|---|
| $l_{hole}$ | 4 | mm |
| $H_{hole}$ | 30 | mm |
| $N_{hole}$ | 8 | – |
| $t_{base}$ | 1 | mm |
| $t_{fin}$ | 3 | mm |
| $N_{fin}$ | 7 | – |
| $k_{f\_c}$ | 0.0257 | W/m K |
| $k_{f\_h}$ | 0.0271 | W/m K |
| $k_s$ | 229 | W/m K |
| $\nu_c$ | 15.11E−06 | $m^2/s$ |
| $\nu_h$ | 16.97E−06 | $m^2/s$ |
| $Pr_c$ | 0.713 | – |
| $Pr_h$ | 0.703 | – |
| $R''$ | 0.001 | $m^2$ K/W |

## 5. Results and discussion

### 5.1. Parametric study and optimization

In this section, the effect of different parameters on performance of the AWG system is studied. In order to optimize the design, an objective function called effectiveness is defined as follows:

$$Eff = \frac{\dot{m}_w}{P_{TEC} + P_{fan}} \tag{39}$$

This indicator represents the amount of produced water relative to the energy consumption of the system. Higher values of this quantity mean that the system consumes less energy to produce the same amount of water. This is an important feature for the systems supplied by solar energy. A system with higher effectiveness needs smaller PV and battery system.

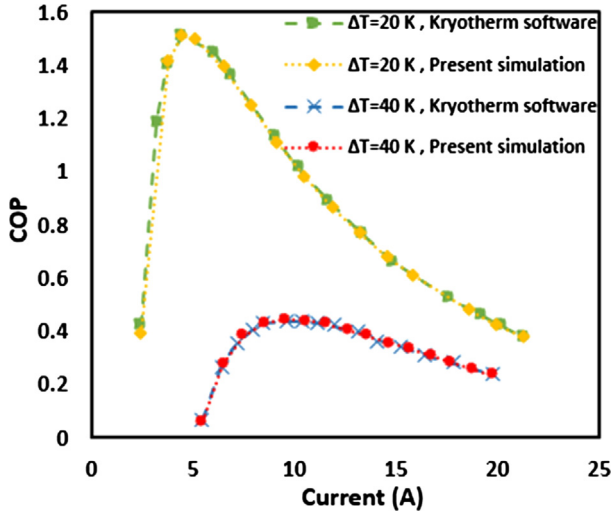


**Fig. 6.** Change of COP vs Current for ΔT = 20K and ΔT = 40K for the considered TEC (KRYOTHERM) [27].

A sensitivity analysis can provide the path for optimization. For instance, Fig. 10 shows the effect of changing electrical current on effectiveness of the system at air flow rate of 0.015 kg/s, ambient temperature of 308 K, relative humidity of 75% and 10 TEC modules placed in a 77 cm long channel. It is observed that by increasing the current, *Eff* first rises and then falls. Therefore, it is very important to supply an

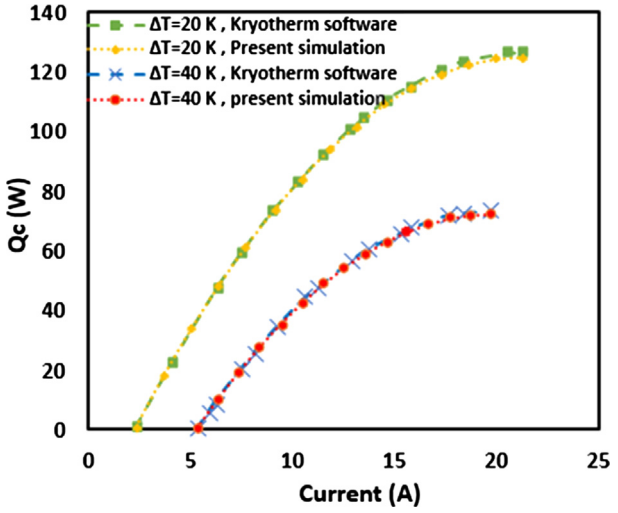


**Fig. 7.** Change of $Q_c$ vs Current for ΔT = 20K and ΔT = 40K for considered TEC (KRYOTHERM) [27].

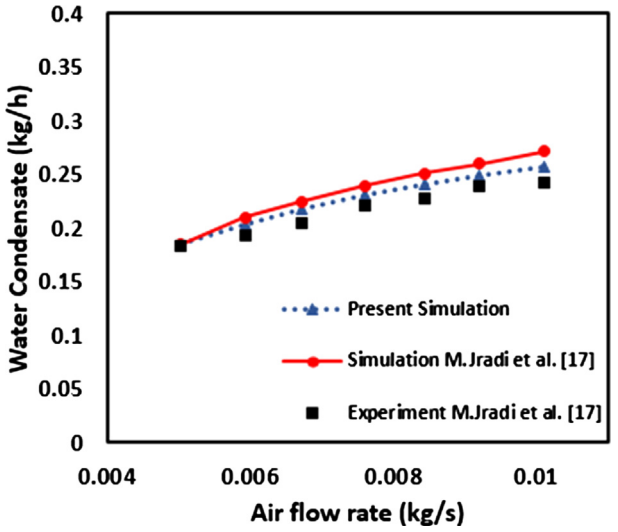


**Fig. 8.** The amount of produced water as a function of air flow.

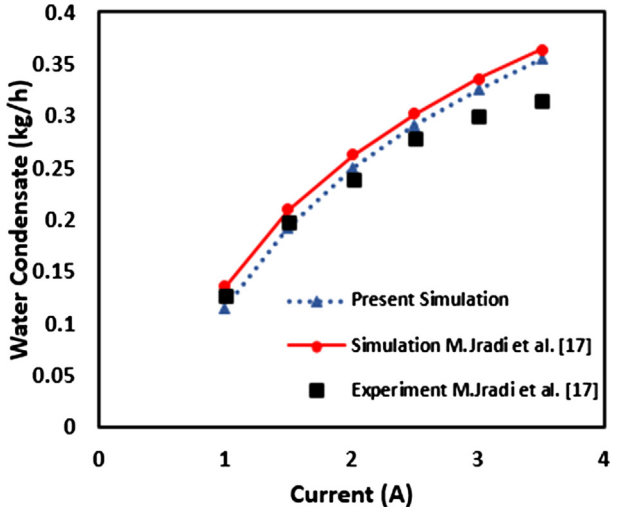


**Fig. 9.** The amount of produced water as a function of electrical current.

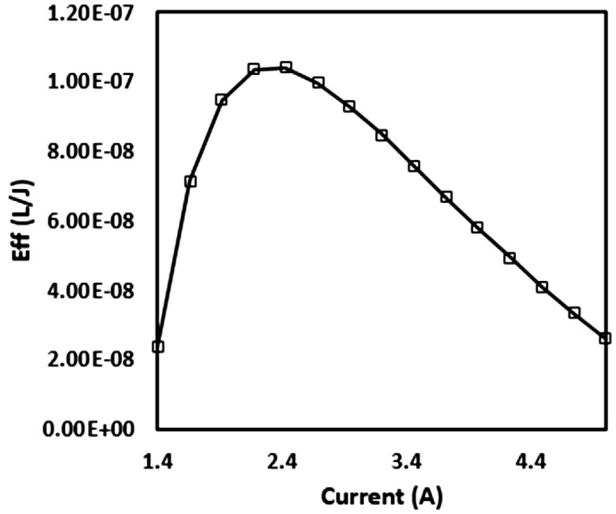


**Fig. 10.** The effect of increasing electric current on the value of effectiveness.

optimum amount of current to the system. However, the optimum value of the current is a function of operating conditions and also the number of thermoelectric coolers.

To find the optimum number of thermoelectric coolers, 15–20 TECs are considered. The length of the channel is proportional to the number of thermoelectric coolers. The ambient condition is assumed to be 308 K with relative humidity of 75%. By changing the electrical currents from zero to $I_{max}$ for $\dot{m}_a$ between 0.01 and 0.02 kg/s, the amount of $Eff_{max}$ is calculated for all cases. Results reported in Table 3 reveal that the maximum effectiveness occurs at COP = 1.9 in all cases. The system with 18 thermoelectric coolers and inlet air flow rate of 0.0117 kg/s has the maximum value of *Eff* which is equal to 1.638E − 07 L/J. Therefore, the optimum length of the channel is 1.386 m with 18 TECs placed in series. This design is used from now on for the study of other parameters.

Effects of changing the electricity current for a channel with the optimum length is shown in Fig. 11. The air flowrate of 0.0117 kg/s, the ambient temperature of 308 K and the relative humidity of 75% are considered. Results reveal that the maximum amount of water production is 42 ml in one hour and it occurs when $I$ = 2.315 A. However, the maximum *Eff* doesn't occur at this point. In fact, $Eff_{max}$= 1.638E − 07L/J is 1.65 times higher than the *Eff* at maximum water production and occurs at I = 1.349 A.

Clearly, the amount of water production is proportional to the relative humidity of the ambient air. Fig. 12 projects this effect for the air flow rate of 0.0117 kg/s and I = 1.349 A. Therefore, it is possible to produce 106 ml of fresh water at high relative humidity within one hour.

To find the optimal performance of the system at different ambient temperatures, the relative humidity of the entering air is considered to be constant and equal to 75%, while the input current to thermoelectric coolers is varied from 0 to $I_{max}$, also air flow rate changes between 0.001 and 0.02 kg/s. The optimum operating mode of the system is calculated for each temperature. These results are reported in Table 4.

Based on the above results:

(1) At the optimal performance, with the increase in entering air temperature, the input electric current to the system decreases. Because when entering air temperature goes higher, the performance range of thermoelectric becomes more limited. If the current exceeds a specific value, the warm side of thermoelectric cooler gets too hot which has a negative effect on its performance. So, for an increase in the entering air temperature, the input current to the system should be decreased.

(2) With the increase in air temperature, the optimal air flow rate is

**Table 3**
Effect of change of number of TECs and length of channel on optimization of the device.

| NO TEC | $I_{channel}$ (m) | $Eff_{max}$ (L/J) | Current (A) | COP | $\dot{m}_a$ (kg/s) | $Re_h$ | $Re_c$ |
|---|---|---|---|---|---|---|---|
| 15 | 1.155 | 1.587E−07 | 1.396 | 1.9 | 0.0109 | 4689 | 4175 |
| 16 | 1.232 | 1.615E−07 | 1.375 | 1.9 | 0.0111 | 4776 | 4252 |
| 17 | 1.309 | 1.632E−07 | 1.369 | 1.9 | 0.0115 | 4950 | 4408 |
| 18 | 1.386 | 1.638E−07 | 1.349 | 1.9 | 0.0117 | 5038 | 4485 |
| 19 | 1.463 | 1.637E−07 | 1.344 | 1.9 | 0.0120 | 5212 | 4641 |
| 20 | 1.54 | 1.629E−07 | 1.336 | 1.9 | 0.0124 | 5343 | 4757 |

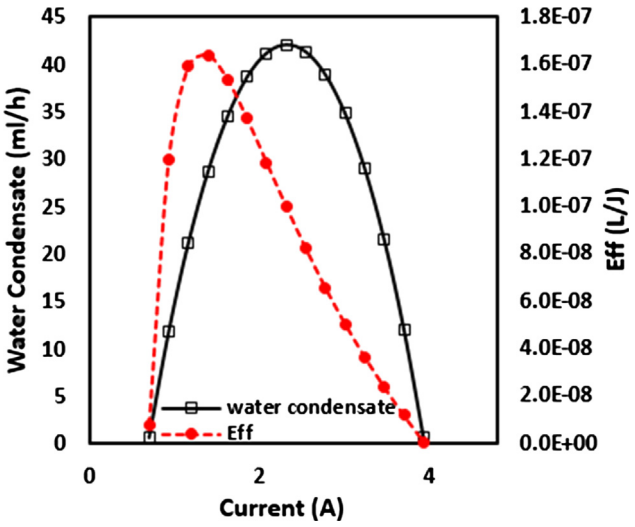


**Fig. 11.** The amount of produced water (in ml/h) as a function of the electric current, at 308 K and 90% relative humidity and air flow rate of 0.0117 kg/s.

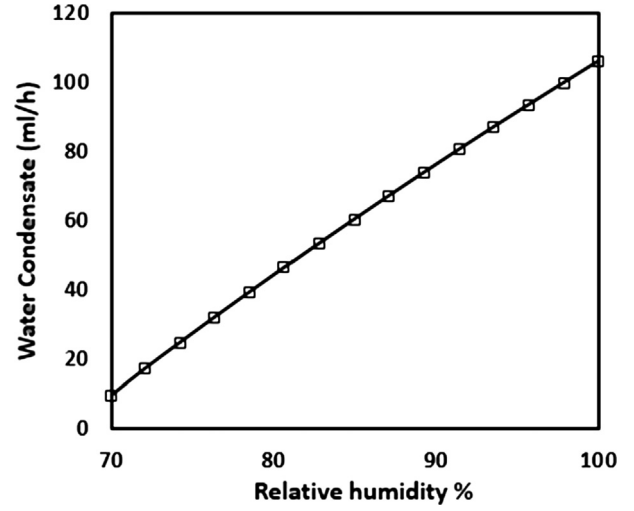


**Fig. 12.** The amount of produced water (in ml/h) as a function of relative humidity, air flow rate of 0.0117 kg/s and I = 1.349 A.

**Table 4**
System optimization results at 75% relative humidity and different inlet temperatures.

| $T_a$ (K) | $\dot{m}_{a\_optimum}$ (kg/s) | Current (A) | COP | $Eff_{max}$ (L/J) |
|---|---|---|---|---|
| 298 | 0.0135 | 1.606 | 1.7 | 1.102E−07 |
| 303 | 0.0127 | 1.485 | 1.8 | 1.299E−07 |
| 308 | 0.0117 | 1.349 | 1.9 | 1.638E−07 |
| 313 | 0.0105 | 1.081 | 2.4 | 2.284E−07 |
| 318 | 0.0084 | 0.758 | 3.2 | 3.684E−07 |

decreased as well, which is justified with the previously discussed observation: by decreasing input current to the system, and therefore decreasing input power to thermoelectric cooler, the generated cooling power also decreases; thus the optimal air flow rate to the system decreases as well, since the cooling power won't be sufficient for higher amounts of flow rate

(3) By increasing the air temperature, $Eff_{max}$ and the COP at which $Eff_{max}$ occurs increase. This is because, with the increase of entering air temperature, the power consumption of thermoelectric cooler also decreases. In addition, the optimum air flow rate and fan power consumption decrease, so the total amount of power consumption decreases, and since warmer air contains more moisture (at the same relative humidity), water production is easier. Therefore, with the increase in temperature, $Eff_{max}$ and COP also increase.

Figs. 13–21 indicate the effect of changing current on water condensation, $Eff$, $T_h$, $T_c$, $\Delta T$, $P_{TEC}$, $Q_h$, $Q_c$ and COP at the optimum air flow rate of each temperature. The effect of current on water production of the system with optimum air flow rate at each temperature is reported in Fig. 13 for the relative humidity of 75%. Based on this figure, the maximum amount of water produced in an hour occurs at 313 K and is equal to 44 ml.

Fig. 14 is also presented to investigate effects of the change in current on the amount of effectiveness. Comparing with Fig. 13, it is clear that the maximum amount of $Eff$ doesn't occur at the current which maximum amount of water is harvested for all cases. It is interesting to note that 26 ml of water can be harvested from the air with 75% relative humidity and 318 K by using only 20 W electrical power within 1 h.

Fig. 15 indicates that by increasing the electrical current, $T_h$ always rises. Also at a fixed current, by increasing the inlet air temperature, the hot side temperature rises and since it's a limiting factor of the system,

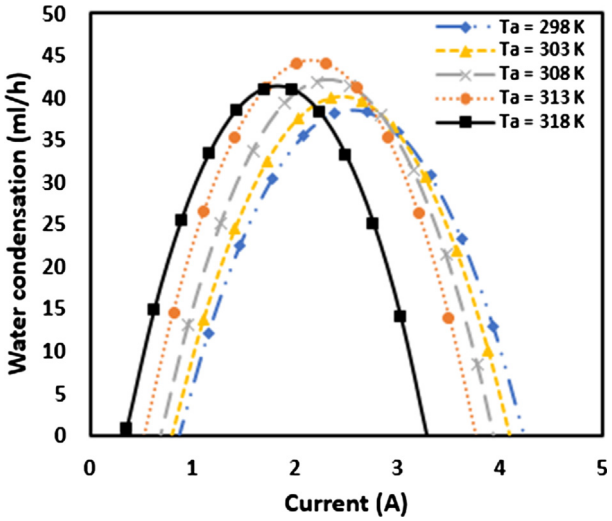


**Fig. 13.** Produced water (in ml/h) as a function of the electric current, at 75% relative humidity for optimum air flow rate at different temperatures.

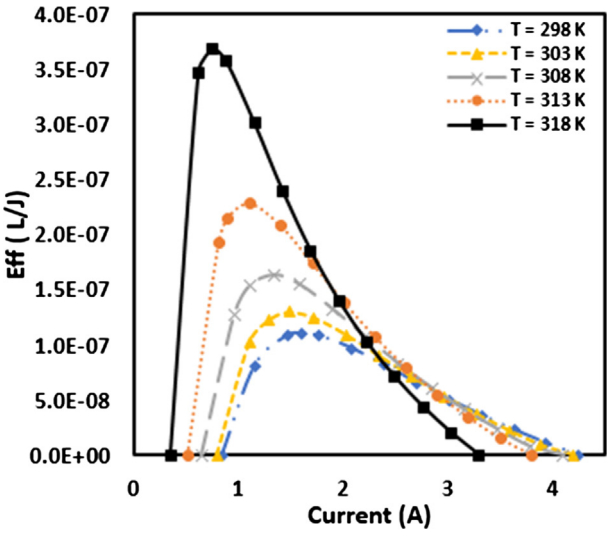


**Fig. 14.** *Eff* as a function of the electric current, at 75% relative humidity for optimum air flow rate of system at different temperatures.

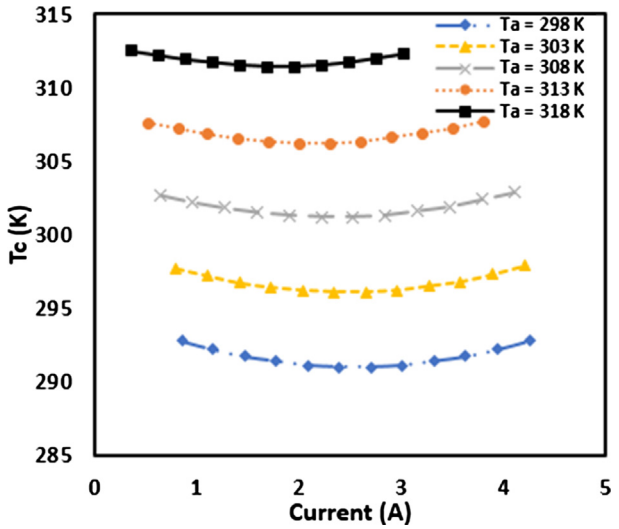


**Fig. 16.** Cold side temperature of TECs as a function of the electric current, at 75% relative humidity for optimum air flow rate of system at different temperatures.

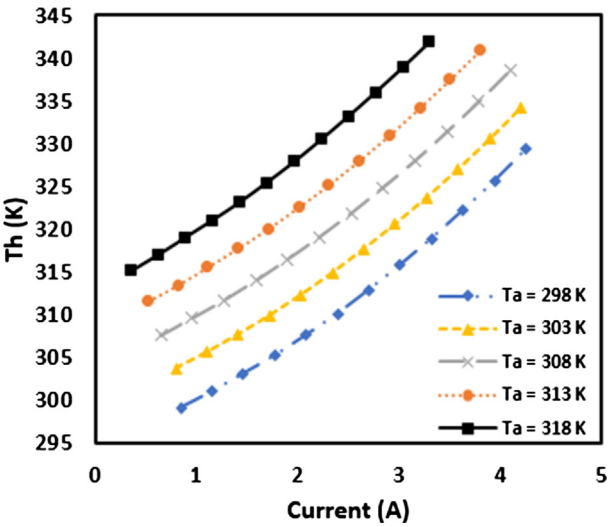


**Fig. 15.** Hot side temperature of TECs as a function of the electric current, at 75% relative humidity for optimum air flow rate at different temperatures.

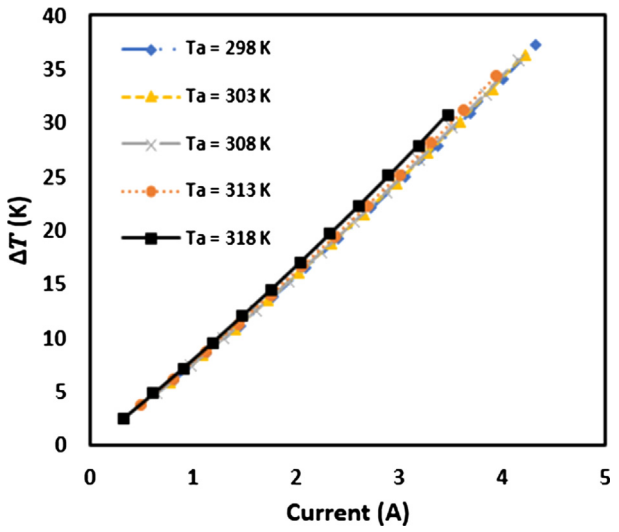


**Fig. 17.** Changes in temperature difference between hot and cold side of TECs as a function of the electric current, at 75% relative humidity for optimum air flow rate of system at different temperatures.

one should be careful about the hot side temperature of TEC in order to prevent damage.

As shown in Fig. 16, by increasing electric current, $T_c$ first falls then rises slightly. The reason is that by increasing current, $T_h$ increases. At first, the optimal flow rate is able to cool the hot side sufficiently and so $T_h$ has a negligible effect on the cold side temperature and $T_c$ decreases as expected. But after a certain current, this optimal flow rate is not able to cool the hot side enough and an increase in the hot side is observed which also results in an increase in $T_c$. However, the range of the change in cold side temperature is not wide, unlike the hot side temperature.

The temperature difference between the hot and cold side ($\Delta T$) has an ascending trend with increasing current as shown in Fig. 17. This behavior is consistent with the previously mentioned change of $T_h$ and $T_c$ with the current. It should be noted that the air inlet temperature has little effect on optimum $\Delta T$.

Fig. 18 indicates that the input power to thermoelectric cooler is approximately the same for all inlet air temperatures and only the performance range of each case is different; it shows that optimum mode of the system occurs at a same thermoelectric cooler's power for different ambient temperatures.

At a fixed current, the rate of heat removal from the hot side of thermoelectric cooler $Q_h$ decreases by increasing inlet air temperature as illustrated in Fig. 19. Because with the increase of inlet air temperature, the optimum inlet air flow rate decreases, so the rate of heat removal from the hot side of thermoelectric cooler decreases.

Also, Fig. 20 demonstrates that the rate of heat transfer from the cold side has an ascending trend at first; and at a specific current, the maximum cooling effect occurs. On the other hand, $Q_c$ decreases with increasing inlet air temperature. The reason is that $Q_c$ depends on $Q_h$ and thermoelectric power and as it was explained before, the optimum amount of input power to TECs is the same in all cases and $Q_h$ decreases with increasing inlet air temperature at a fixed current. So $Q_c$ must be reduced with warmer inlet air at a fixed current.

Finally, Fig. 21 shows that at a fixed current, COP falls with the increase of inlet air temperature. The reason is that $Q_c$ decreases while the power consumption $P$ doesn't change significantly with increasing inlet air temperature.

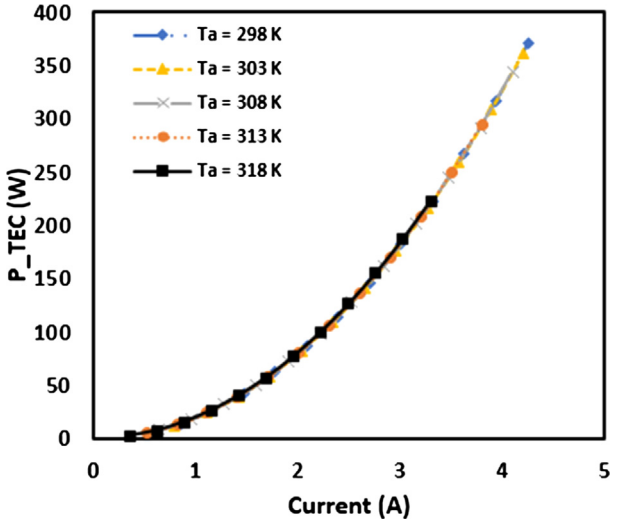


**Fig. 18.** Input power to TECs as a function of the electric current, at 75% relative humidity for optimum air flow at different temperatures.

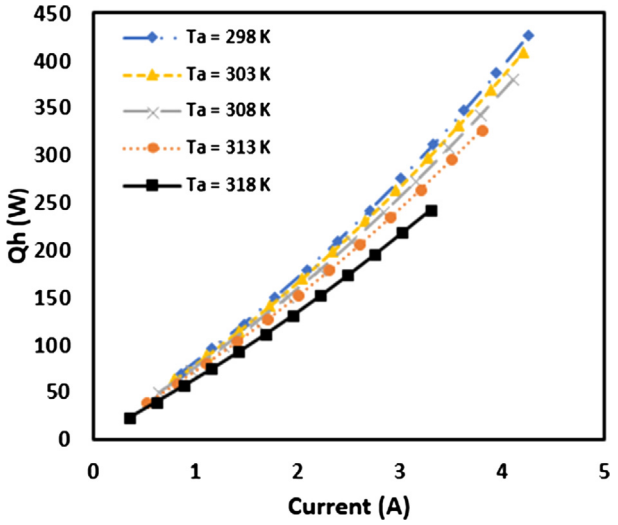


**Fig. 19.** Heat removal from hot side of TECs as a function of the electric current, at 75% relative humidity for optimum air flow rate of system at different temperatures.

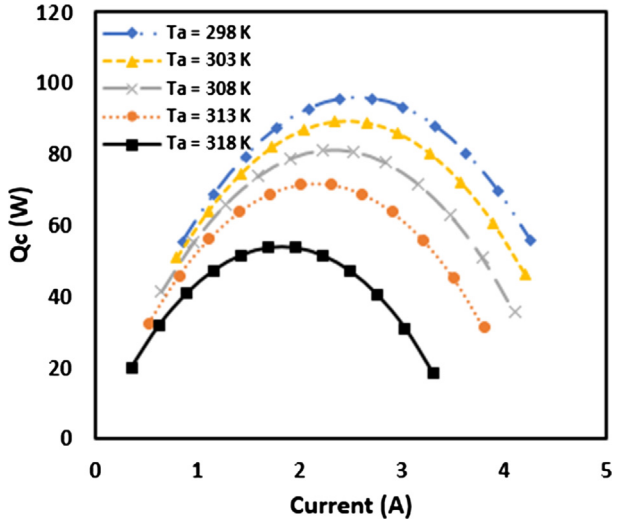


**Fig. 20.** Heat removal from the cold side of TECs as a function of the electric current, at 75% relative humidity for optimum air flow rate of system at different temperatures.

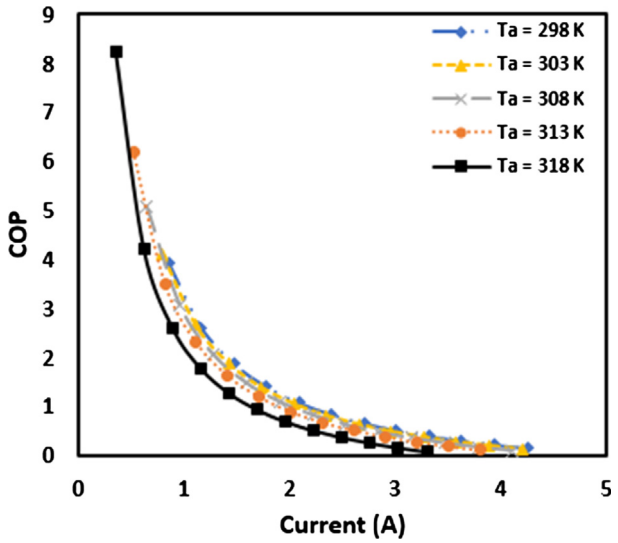


**Fig. 21.** Changes in coefficient of performance of TECs as a function of the electric current, at 75% relative humidity for optimum air flow rate of system at different temperatures.

### 5.2. Annual performance in three southern cities of Iran

In this section, the annual amount of water condensation and energy consumption is calculated for three southern cities of Iran. All these three cities are faced with the problem of water scarcity. Also, they are proper candidates to evaluate the proposed system, since they are in the vicinity of the sea and therefore, have high values of relative humidity. For this purpose, hourly weather data for Kish island, Bandar-e-Abbas and Bandar-e-chabahar are obtained via Iran meteorological organization [31] for the duration of one year.

At first, it is assumed that the system is always on, with a constant electrical current and air flow rate supplied. Although the optimum values of these two controlling parameters were found in the previous section for different inlet temperatures, the ambient condition is variable during a year. Therefore, now the question is that what electrical current and air flow rate results in the best yearly performance?

To find the answer, the effect of changing electrical current on yearly effectiveness is demonstrated in Fig. 22 for Kish island. The optimum electrical current at each flow rate is lower than what was found in the previous section for the corresponding fixed inlet temperature. Again, higher annual *Eff* can be achieved by reducing the air flow rate. However, less water is produced if a lower air flow rate is supplied by the fan as illustrated in Fig. 23. It shows the effect of current on water condensation during 1 year for different air flow rates. The interesting point is that the optimum current for maximum production in a year is almost the same as the value found in the previous section for a fixed inlet temperature. Therefore, the variable ambient condition has a little effect on the optimum current at the desired flow rate for maximum production.

Taking a closer look at the results, it is found that the system with constant electrical current is not capable of producing water in almost half of the year. Therefore, a wise decision is to turn off the system in these times for energy saving purposes. In fact, a fundamental advantage of the present analysis is that it can predict the possibility of producing water for different values of relative humidity and temperature. If a controller is used to turn the system off and on, then the same amount of water is gained with higher effectiveness.

To study the behavior of the on/off system, water condensation, power consumption (kWh) and effectiveness is calculated during one

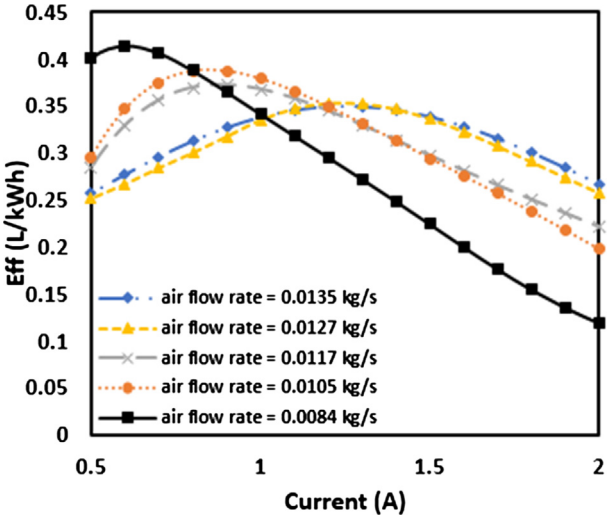


**Fig. 22.** *Eff* (in L/kWh) as a function of the electric current, at different mass flow rate for Kish island during 1 year; The system is always on.

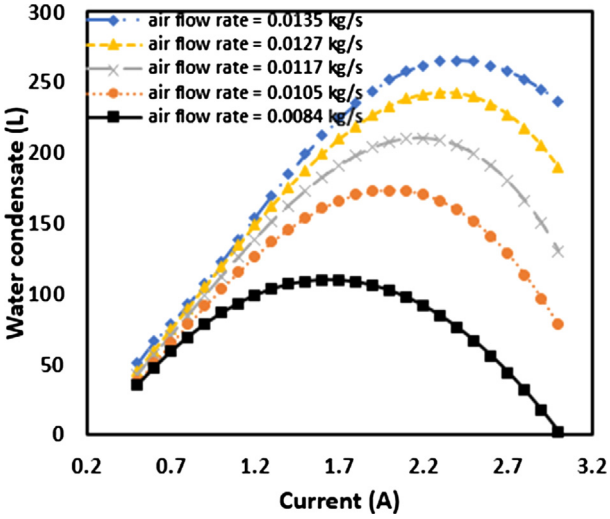


**Fig. 23.** Water condensation as a function of the electric current, at different mass flow rate for Kish island during 1 year.

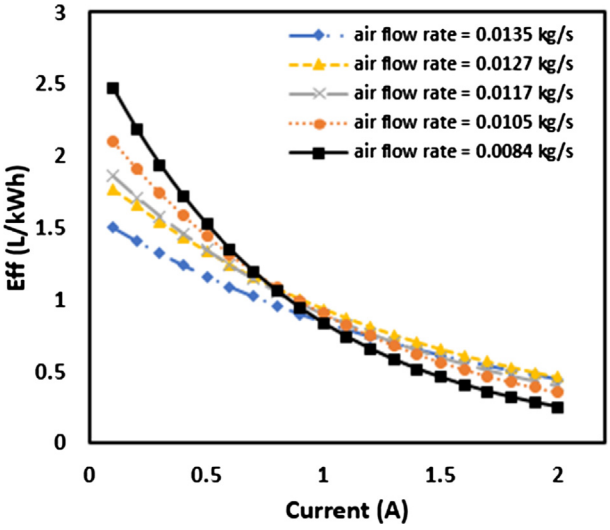


**Fig. 24.** *Eff* as a function of the electric current, at different mass flow rate for Kish island during 1 year. The system is on/off.

year for Kish island at different electrical currents and air flow rates. Fig. 24 shows that the effectiveness of the on/off system falls as the supplied electrical current increases. Unlike the always-on case, one cannot find an optimum current for maximum effectiveness. The reason is that during a year, there are times that the ambient relative humidity is very high. In these periods, it is possible to produce water with very small values of electrical current. Such a system is shut down most of the time and produces a small amount of water very efficiently.

Therefore, the objective function for optimization of the yearly performance of the on/off system can be the total amount of water production which is the same as the maximum value found in Fig. 23. As expected, more water can be harvested with higher air flow rates, although with lower effectiveness. Table 5 summarizes the annual performance of the system. It is interesting that the on/off system can produce larger amounts of fresh water than the always-on device with approximately the same effectiveness. Also, the same amount of water can be harvested much more efficiently if the system can be switched off while there is no water production.

Similarly, the amount of water production, power consumption and effectiveness for two other cities of Bandar-e-Abbas and Bandar-e-chabahr are investigated for $\dot{m}_a$ = 0. 0117 kg/sand I = 0.9 A and I = 2.1 A. Results are compared with Kish islands in Figs. 25 and 26.

According to Fig. 25, power consumption for all three cities is approximately the same if the system is always on. However, the amount of water condensation in Bandar-e-chabahar is much higher and thereby the highest *Eff* among the three cities occurs for this location which is equal to 0.533 L/kWh. Also, when the system is on/off, the highest *Eff* is for Kish island. The reason is that the electrical current of I = 0.9 A is the optimum value obtained based on the annual weather data of this city. Also, Fig. 26 shows that the maximum amount of water condensation during 1 year (312 L) is produced in Bandar-e-chabahar which has higher relative humidity compared to two other cities.

### 5.3. Comparison between the present design and other AWG systems

Finally, the specific energy consumption (which is the energy consumption (kWh) for condensation of 1 $m^3$ of water) for different AWG systems proposed in the literature is compared in Table 6.

It is found that the present design is the most energy efficient system among similar devices proposed in the literature. The reason is that different operating parameters are considered simultaneously in the present optimization. However, the effectiveness of the present system is not competitive at lower values of relative humidity. Because the optimizations are performed for 75% relative humidity, if the system is intended to work at lower relative humidity, one should optimize the system again to have better performance. Also, it is important to note that the ambient relative humidity greatly affects the specific energy consumption. For example, a 5% increase in relative humidity can decrease the specific energy consumption by about 50%. Also by comparison between present work and the commercial system using a vapor compression refrigeration cooling [32], it can be seen that in high relative humidity, the present design is even marginally performing better.

## 6. Conclusion

In this study, thermodynamic analysis and optimization of a device for water harvesting from humid air is presented. Air cooling is achieved by a number of thermoelectric coolers. All of the necessary geometrical, meteorological, technical and thermophysical parameters are taken into account to have an accurate estimate of the actual system behavior, including thermal resistances and fins geometry. Optimizations were performed to obtain fresh water with minimum possible energy consumption. According to the results, 18 TECs in a channel with the length of 1.386 m has the best *Eff* among the cases investigated. Optimal electrical current and air flow rate were

**Table 5**
Annual performance of the system in Kish island for different air mass flow rates.

| | The system is always on | | | | | The system is on/off | | | | |
|---|---|---|---|---|---|---|---|---|---|---|
| | $\dot{m}_a$ (kg/s) | | | | | $\dot{m}_a$ (kg/s) | | | | |
| | 0.0135 | 0.0127 | 0.0117 | 0.0105 | 0.0084 | 0.0135 | 0.0127 | 0.0117 | 0.0105 | 0.0084 |
| Maximum water condensation (L) | 265.4 | 241.2 | 209.7 | 173.8 | 112.4 | 265.4 | 241.2 | 209.7 | 173.8 | 112.4 |
| Water condensation at $Eff_{max}$ (L) | 153.59 | 147.57 | 98.03 | 91.12 | 46.98 | n/a | n/a | n/a | n/a | n/a |
| $I$ at maximum water condensation (A) | 2.4 | 2.2 | 2.1 | 1.9 | 1.6 | 2.4 | 2.2 | 2.1 | 1.9 | 1.6 |
| $I$ at $Eff_{max}$ (A) | 1.2 | 1.2 | 0.9 | 0.9 | 0.6 | 0 | 0 | 0 | 0 | 0 |
| Power consumption at maximum water condensation (kWh) | 1289.91 | 1086.61 | 1020.02 | 793.75 | 560.83 | 784.94 | 652.02 | 572.72 | 450.95 | 281.77 |
| Power consumption at $Eff_{max}$ (kWh) | 431.05 | 409.40 | 260.52 | 235.37 | 114.01 | 0 | 0 | 0 | 0 | 0 |
| Power consumption at $Eff_{max}$ of system when is always on (kWh) | The same as Power consumption at $Eff_{max}$ (kWh) for each air flow rate | | | | | 201.21 | 192.97 | 99.35 | 92.07 | 33.61 |
| $Eff$ at Maximum water condensation (L/kWh) | 0.206 | 0.222 | 0.206 | 0.219 | 0.200 | 0.338 | 0.370 | 0.366 | 0.385 | 0.400 |
| $Eff_{max}$ (L/kWh) | 0.356 | 0.360 | 0.376 | 0.387 | 0.412 | ∞ | ∞ | ∞ | ∞ | ∞ |
| $Eff$ for $I$ at $Eff_{max}$ of the always on (L/kWh) | The same as $Eff_{max}$ for each air flow rate | | | | | 0.763 | 0.765 | 0.987 | 0.990 | 1.400 |

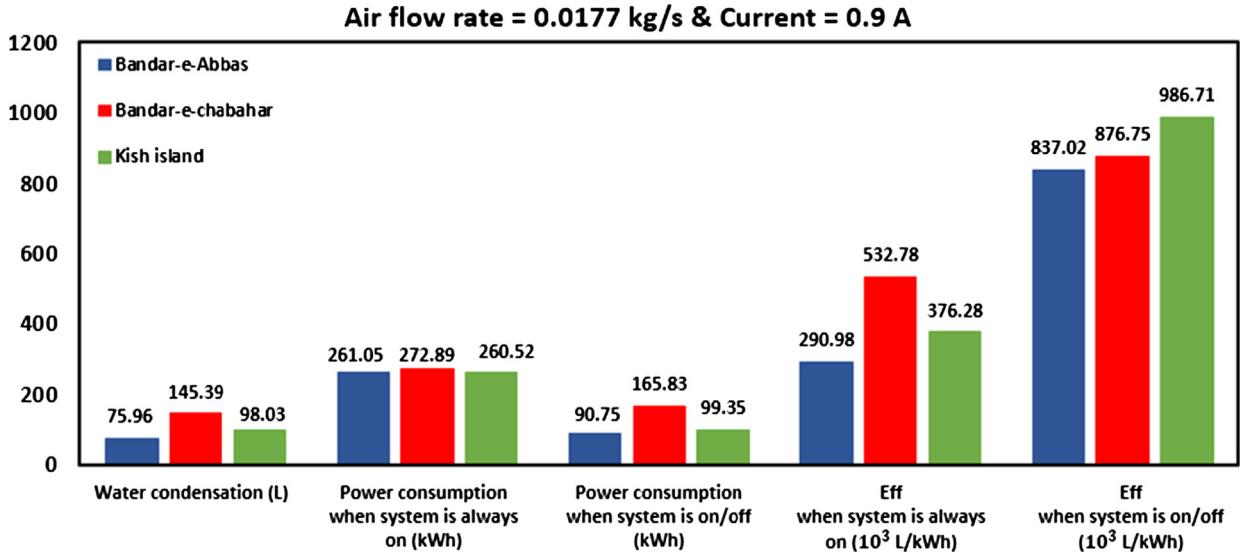


**Fig. 25.** Annual water production, power consumption and effectiveness for three locations for duration of 1 year at air flow rate of 0.0117 kg/s and I = 0.9 A.

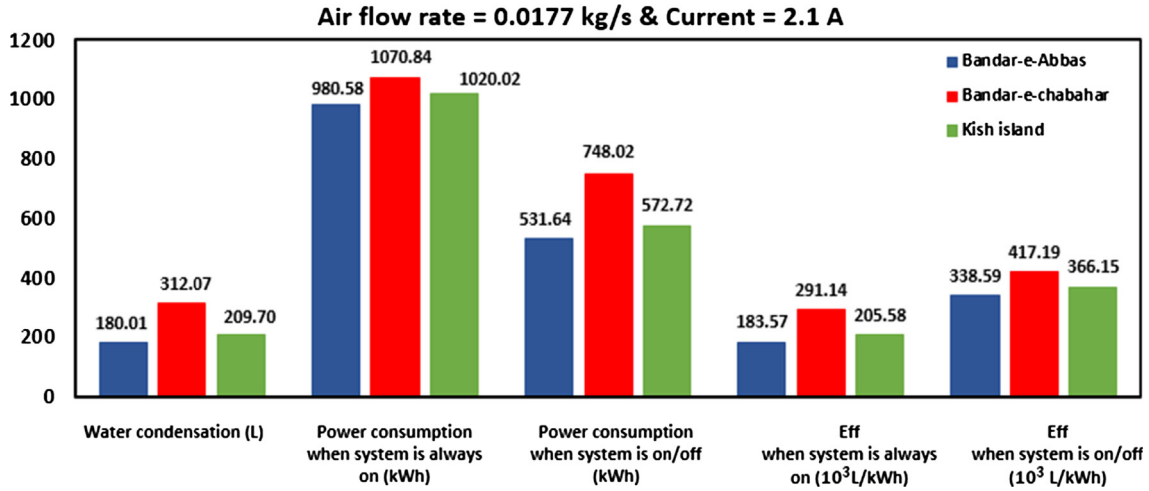


**Fig. 26.** Annual water production, power consumption and effectiveness for three locations for duration of 1 year at air flow rate of 0.0117 kg/s and I = 2.1 A.

calculated for different inlet air temperature. It was found that these two controlling parameters should be decreased at higher air temperatures. The system is capable of harvesting 26 ml of water from the air with 75% relative humidity and 318 K by using only 20 W power within 1 h.

Also, the annual performance of this device in three southern cities in Iran (Kish island, Bandar-e-Abbas and Bandar-e-chabahar) were investigated for two modes of operation: the always-on and on/off

**Table 6**
Specific energy consumption (in kWh/m$^3$) for the present work and other AWG systems.

| System | Specific energy consumption (kWh/m$^3$) | $T_a$ (K) | Relative humidity % | Comments |
|---|---|---|---|---|
| Present work | 252.78 | 303 | 90 | – |
| Present work | 489.95 | 306 | 85 | – |
| Present work | 911.57 | 306 | 80 | – |
| Present work | 769.23 | 318 | 75 | – |
| Present work | 22336.38 | 318 | 60 | – |
| Present work | 1013.47 | Kish island climate | Kish island climate | The system is on/off |
| Present work | 1876.95 | Bandar-e-chabahar climate | Bandar-e-chabahar climate | The system is always on |
| Tan and Fok [21] | 7294.11 | 302 | 79 | – |
| Shanshan Liu et al. [22] | 2318.72 | 296.6 | 92.7 | – |
| Pontious et al. [24] (Peltier) | 1571.43 | – | – | Exact data for climate condition is not available |
| Shourideh et al. [25] | 2002.00 | 303 | 60 | At the first hour of test (unsteady) |
| Shourideh et al. [25] | 1870.00 | 303 | 60 | At the second hour of test (steady) |
| Shourideh et al. [25] | 936.00 | 306 | 80 | At the first hour of test (unsteady) |
| Shourideh et al. [25] | 922.00 | 306 | 80 | At the second hour of test (steady) |
| Commercial AWG system [32] | 257.18 | 303 | 90 | Ambient water group (vapor compression refrigeration) |
| Commercial AWG system [33] | 410 | 303 | 80 | EcoloBlue group (vapor compression refrigeration) |

system. Results reveal that there is no optimum electrical current for the effectiveness of the on/off system. Among the three locations considered, Bandar-e-chabahar has the highest yearly yield because of higher ambient air relative humidity. In the end, a comparison between this device and other air water generators indicates that present design is the most energy efficient system among similar devices; especially in high relative humidity.

## References


[1] Claire S. The Last Drop. Mazaya, Summer Issue; 2002. p. 22–5.
[2] Mekonnen MM, Hoekstra AY. Four billion people facing severe water scarcity. Sci Adv 2016;2(2):e1500323.
[3] Zhao D, Tan G. A review of thermoelectric cooling: materials, modeling and applications. Appl Therm Eng 2014;66(1–2):15–24.
[4] Fraisse G, Ramousse J, Sgorlon D, Goupil C. Comparison of different modeling approaches for thermoelectric elements. Energy Convers Manage 2013;65:351–6.
[5] Mani PI. Design, modeling and simulation of a thermoelectric cooling system (TEC); 2016.
[6] Enescu D, Virjoghe EO. A review on thermoelectric cooling parameters and performance. Renew Sustain Energy Rev 2014;38:903–16.
[7] Xuan XC. Investigation of thermal contact effect on thermoelectric coolers. Energy Convers Manage 2003;44(3):399–410.
[8] Cosnier M, Fraisse G, Luo L. An experimental and numerical study of a thermoelectric air-cooling and air-heating system. Int J Refrig 2008;31(6):1051–62.
[9] Liu ZB, Zhang L, Gong G, Luo Y, Meng F. Experimental study and performance analysis of a solar thermoelectric air conditioner with hot water supply. Energy Build 2015;86:619–25.
[10] Dizaji HS, Jafarmadar S, Khalilarya S, Moosavi A. An exhaustive experimental study of a novel air-water based thermoelectric cooling unit. Appl Energy 2016;181:357–66.
[11] Seo YM, Ha MY, Park SH, Lee GH, Kim YS, Park YG. A numerical study on the performance of the thermoelectric module with different heat sink shapes. Appl Therm Eng 2018;128:1082–94.
[12] Vian JG, Astrain D. Development of a heat exchanger for the cold side of a thermoelectric module. Appl Therm Eng 2008;28(11–12):1514–21.
[13] Zhu L, Tan H, Yu J. Analysis on optimal heat exchanger size of thermoelectric cooler for electronic cooling applications. Energy Convers Manage 2013;76:685–90.
[14] Tan H, Fu H, Yu J. Evaluating optimal cooling temperature of a single-stage thermoelectric cooler using thermodynamic second law. Appl Therm Eng 2017;123:845–51.
[15] Tan FL, Fok SC. Methodology on sizing and selecting thermoelectric cooler from different TEC manufacturers in cooling system design. Energy Convers Manage 2008;49(6):1715–23.
[16] Vián JG, Astrain D, Domınguez M. Numerical modelling and a design of a thermoelectric dehumidifier. Appl Therm Eng 2002;22(4):407–22.
[17] Jradi M, Ghaddar N, Ghali K. Experimental and theoretical study of an integrated thermoelectric–photovoltaic system for air dehumidification and fresh water production. Int J Energy Res 2012;36(9):963–74.
[18] Yao Y, Sun Y, Sun D, Sang C, Sun M, Shen L, et al. Optimization design and experimental study of thermoelectric dehumidifier. Appl Therm Eng 2017;123:820–9.
[19] Atta RM. Solar water condensation using thermoelectric coolers. Int J Water Resour Arid Environ 2011;1(2):142–5.
[20] Joshi VP, Joshi VS, Kothari HA, Mahajan MD, Chaudhari MB, Sant KD. Experimental investigations on a portable fresh water generator using a thermoelectric cooler. Energy Proc 2017;109:161–6.
[21] Tan FL, Fok SC. Experimental testing and evaluation of parameters on the extraction of water from air using thermoelectric coolers. J Test Eval 2012;41(1):96–103.
[22] Liu S, He W, Hu D, Lv S, Chen D, Wu X, et al. Experimental analysis of a portable atmospheric water generator by thermoelectric cooling method. Energy Proc 2017;142:1609–14.
[23] Muñoz-García MA, Moreda GP, Raga-Arroyo MP, Marín-González O. Water harvesting for young trees using Peltier modules powered by photovoltaic solar energy. Comput Electron Agric 2013;93:60–7.
[24] Pontious K, Weidner B, Guerin N, Pierrakos O, Altaii K. Design of an atmospheric water generator: Harvesting water out of thin air. In: Systems and information engineering design symposium (SIEDS); 2016. p. 6–11.
[25] Shourideh AH, Ajram WB, Al Lami J, Haggag S, Mansouri A. A comprehensive study of an atmospheric water generator using Peltier effect. Therm Sci Eng Prog 2018;6:14–26.
[26] Salek F, Moghaddam AN, Naserian MM. Thermodynamic analysis and improvement of a novel solar driven atmospheric water generator. Energy Convers Manage 2018;161:104–11.
[27] Informational booklet. Kryotherm, http://kryothermtec.com/catalogs.html/; 2017 [accessed 2 July 2017].
[28] Liu Z, Zhang L, Gong G. Experimental evaluation of a solar thermoelectric cooled ceiling combined with displacement ventilation system. Energy Convers Manage 2014;87:559–65.
[29] Cengel YA, Boles MA. Thermodynamics: an engineering approach. 8th ed. New York: McGraw-Hill; 2015.
[30] Bergman TL, Incropera FP, DeWitt DP, Lavine AS. Fundamentals of heat and mass transfer. 7th ed. New York: John Wiley & Sons; 2011.
[31] IRIMO REPORT Server; 2018. http://reports.irimo.ir/jasperserver/login.html/ [accessed 15 March 2018].
[32] Ambient Water Systems; 2018. http://www.ambientwater.com/en/systems/ [accessed 28 March 2018].
[33] EcoloBlue Water from Air; 2018. http://ecoloblue.com/ecoloblue-1000/47-ecoloblue-1000.html/[accessed 28 March 2018].